TASK QUARTERLY 5 No 4 (2001), 557–566

INSTABILITY OF THE NON-ISOTHERMAL FLOW BETWEEN A ROTATING AND A STATIONARY DISKS

EWA TULISZKA-SZNITKO[1], CHYI-YEOU SOONG[2], ERIC SERRE[3] AND PATRICK BONTOUX[3]

[1]*Institute of Thermal Engineering, Technical University of Poznań, Piotrowo 3, 60-965 Poznań, Poland*
sznitko@sol.put.poznan.pl

[2]*Rotating Fluids and Vortex Dynamics Laboratory, Department of Aeronautical Engineering, Chung Cheng Institute of Technology, Tahsi, Taoyuan, Taiwan 33509, Republic of China*

[3]*Laboratoire de Modélisation et Simulation Numérique en Mécanique, LABM/CNRS, IMT Château-Gombert, La Jetée, Université de la Méditerranée, F. Joliot-Curie 38, 13451 Marseille Cedex 20, France*

(Received 31 July 2001; revised manuscript received 15 August 2001)

Abstract: Both theoretical linear stability analysis and the direct numerical simulation are performed to study the transition flow between rotating discs. This paper reports about the three-dimensional spiral and annular patterns computed with a high-order (spectral) numerical method in the Bödewadt layer of a cylindrical rotor/stator cavity. The characteristic parameters of these boundary layer instabilities are compared with the theoretical results and interpreted in terms of type I and type II generic instabilities. The absolute instability regions are theoretically identified and the critical Reynolds numbers of the convective/absolute transition in both layers are given. The absolute or convective nature of the flows is determined by examining the branch-points singularities of the dispersion relation.

Keywords: instability and transition in rotating flows, convective and absolute instability

1. Introduction

The investigation of the laminar-turbulent transition process inside the inter-disc three-dimensional rotating flow is of great interest for the internal aerodynamics of engines, especially for the optimization of turbomachinery air-cooling devices.

In the past decades, numerous works have been devoted to the investigation of the flow structure and to the instabilities associated to the single rotating-disc [1–3] and to the differentially rotating discs [4–7]. Non-isothermal flow conditions have also

been considered [6], showing that the thermal effects and the rotation-induced buoyancy become influential on the stability characteristics and on the critical conditions. All these investigations revealed that for sufficiently high rotation rate, the primary bifurcation occurs in the boundary layers of the Batchelor flow, composed of two different boundary layers close to the discs (Ekman and Bödewadt type close to the rotating and the stationary disc, respectively) and separated by an inviscid geostrophic core. Two basic types of the linear instability for co-rotation of the fluid and the disc, referred to as type I and type II, have been documented both experimentally and theoretically. The type I instability (also referred to as a "crossflow" instability observed in the flow over a swept wing) is due to the presence of an unstable inflection point in the boundary layer velocity profile. The mechanism for type II instability is related to the combined effects of Coriolis and viscous forces. The onset of the type II instability corresponds to a lower local critical Reynolds number than for type I [8]. The convective nature of spirals in the Ekman layer has been experimentally demonstrated by studying the response of the flow over a single rotating disc to a local perturbation [3]. In addition, the convective/absolute nature of the transition in the boundary layer flow over a single rotating disc has been evidenced in both theoretical and experimental studies [2, 3]. For the rotating flow over an infinite stationary disc, Lingwood [9] also found theoretically the existence of this convective/absolute transition. The recent experimental results of the instability of the flow between a stationary and a rotating disc, have also revealed that the flow exhibits a convective/absolute transition in a rotor/stator cavity [10].

In the present paper, we investigate more precisely the character of boundary layer instabilities in the viscous flow between two coaxial rotating discs. A linear stability theory (LST) is performed in order to enlighten the numerical results obtained in a cylindrical rotor/stator cavity in terms of type I and type II instabilities. The characteristic parameters of the annular and spiral patterns exhibited by direct numerical simulation (noted DNS) are shown to be in good agreement with the theoretical results corresponding to the I and II type generic instabilities. The absolute instability regions are theoretically identified, extending the approach of Lingwood [2, 3, 9] for a single disc to the case of the rotor/stator flow.

2. Geometrical and mathematical models

The geometrical model is a rotor/stator cylinder of radius R. Using LST, R is considered to be infinite, whereas in the case of the direct numerical approach the discs are bounded by a stationary cylinder of height 2h (called the shroud). The rotor (upper disc) rotates at uniform angular velocity $\Omega = \Omega e_z$, e_z being the unit vector on the axis. The equations governing the flow are the 3D Navier-Stokes equations written in velocity-pressure formulation, together with the continuity equation and appropriate boundary and initial conditions. It is convenient to write these using a cylindrical polar coordinate system (r, z, φ), relative to a stationary observer with the origin at the centre of the cylinder. The scales for the dimensionless variables of space, time and velocity are h, Ω^{-1}, ΩR, respectively. The two dimensionless parameters that characterise the problem are the Reynolds number $\mathrm{Re} = \Omega(2h)^2/\upsilon$ and the aspect ratio $L = R/2h$ (in the case of confined cavity).

3. Direct numerical simulation (DNS)

The numerical solution is based on a pseudospectral collocation Chebyshev-Fourier Galerkin method. The use of the Gauss-Lobatto collocation points in the radial and axial

directions, directly ensures high accuracy of the solution inside the very narrow wall layers. The time scheme is semi-implicit and second-order accurate. It corresponds to a combination of the second-order backward differentiation formula for the viscous diffusion term and the Adams-Bashforth scheme for the nonlinear terms. The velocity-pressure coupling is performed with an improved projection algorithm [11]. A dependent variable transformation is introduced in order to deal with the lack of physical boundary condition at the axis in the case of the first Fourier axisymetric mode as proposed by Serre and Pulicani [11]. The disturbance equations are obtained by writing the velocity, temperature and pressure fields, as a superposition of the basic state and a perturbation field.

4. Linear stability theory (LST)

The disturbance equations are obtained by expressing the velocity and the pressure fields, as a superposition of the basic state and a perturbation field. We assume the flow to be locally parallel and the perturbation quantities have the following normal-mode form:

$$[u', v', w', p']^T = [\hat{u}, \hat{v}, \hat{w}, \hat{p}]^T \exp(\alpha^* r^* + m\varphi - \omega^* t^*) + cc, \tag{1}$$

where $\hat{u}$, $\hat{v}$, $\hat{w}$, $\hat{p}$ are the dimensional amplitudes of three components of velocity (in r^*, z^*, φ directions) and pressure respectively, α^* and $\beta^* = m/r^*$ are the components of wave number k^* in the radial and circumferential directions, respectively, ω^* is the frequency and t^* is time. Asterisks denote the dimensional values. The linear stability theory equations plus the homogenous boundary conditions create an eigenvalue problem which is solved with a global manner [6]. As in the direct numerical approach, a spectral collocation method based on Chebyshev polynomials is used for discretisation of the LST equations.

To check the character of instability, the flow is impulsively exited at a certain location in space and time. The response of the boundary layer shows whether the flow is absolutely or convectively unstable. The flow is defined as absolutely unstable if its impulse response grows with time at every location in space [12]. If the response decays at every location in sufficiently large time, the flow is convectively unstable. The response of a linear system to the forcing input can be determine by the Green function $G(x,t)$:

$$G(x,t) = \frac{1}{(2\pi)^2} \int_F \int_L \frac{e^{i(kx-\omega t)}}{D(k,\omega;\mathrm{Re}_\delta)}\, d\omega\, dk, \tag{2}$$

where path F in the complex plane of wave number k is initially taken to be the real axis. The contour L in the complex frequency plane ω is chosen so that the causality is satisfied: $G(x,t) = 0$ everywhere when $t < 0$. In most cases the Fourier-Laplace integral (2) cannot be evaluated for arbitrary chosen time; however, for a general dispersion relation one may obtain the time asymptotic Green function. From this asymptotic solution a general mathematical criterion based on the properties of the dispersion relation in complex k and ω planes has been derived to determine the nature of instability [12]. According to this criterion the absolute instability can be identified by singularities in the dispersion relation called pinch-points. The pinch-points are located in a process of consecutive contour deformations in which L is deformed toward the lower half of the ω plane [13]. We have the following criteria for absolute instability. The flow is absolutely unstable if so called absolute amplification rate ω_{oi} is positive ($\omega_{oi} > 0$). Additionally, for contour L located high enough in the ω plane the spatial branches $k^+(\omega)$ and $k^-(\omega)$ must lie in different halves of the k plane.

5. Numerical results. Annular and spiral patterns in a Bödewadt layer

The chosen aspect ratios are $L = 2$ and $L = 5$. The numerical strategy consists in increasing step by step the rotation rate from the base steady state to more complex flow regimes. Due to the nonlinear effects close to the axis, the grid refinement is rather important: $N \times M \times K = 64 \times 64 \times 48$, $123 \times 123 \times 48$ for $\mathrm{Re} = 4000$, $L = 2$ and $123 \times 33 \times 48$ for $\mathrm{Re} = 1600$ and $L = 5$. The time-step incorporated is $\delta t = 10^{-3}$ (Serre and Pulicani [11]).

5.1. Axisymmetric instability

The annular patterns occur on the stator disc only – the Ekman layer on the rotating disc remains stable – for $\mathrm{Re} = 4000$, $L = 2$ and $\mathrm{Re} = 1600$, $L = 5$. For the aspect ratio $L = 2$, a Hopf bifurcation is observed and the angular frequency $\sigma = \omega^*/\Omega = 0.9$ is very close to the rotation frequency ($\sigma = 1$). This solution is characterised by four to five pairs of circular vortices with a radial wavelength $10 \leq \lambda_r^*/\delta \leq 21$ increasing with the radius, where $\delta = \sqrt{\nu/\Omega}$. These vortices travel inward (indicated by a negative speed velocity) along the Bödewadt layer with a phase velocity varying over the range $-0.08 \leq V_\phi^*/\Omega r^* \leq -0.02$ (V_ϕ^* being measured from numerical solutions), to a local radius, corresponding to a local Reynolds number $\mathrm{Re}_\delta = 21$ ($\mathrm{Re}_\delta = r^*/\delta$), where they completely disappear. For the larger aspect ratio $L = 5$, the solution is time-dependent with a primary frequency $\sigma = 4$ and characterised by vortices of the radial wavelength $8 \leq \lambda_r^*/\delta \leq 17$ that vanish at $\mathrm{Re}_\delta = 27$.

5.2. Three-dimensional instability

The three-dimensional flow was obtained by using as an axisymmetric solution and a three-dimensional perturbation of general form $\tilde{\alpha}\sin(p\phi)$ the initial condition: p is an arbitrary number corresponding to an azimuthal wavelength and $\tilde{\alpha}$ is the amplitude rate of typical value 0.05 [7]. The orientation of the wave front is measured in terms of the angle ε with respect to the azimuthal direction of the geostrophic flow and is defined positive when inclined towards the axis. The wavelength of the spiral patterns can be defined by λ^*, as $\lambda^* = (2\pi r^*/n)|\sin\varepsilon|$, where n is the number of arms over 2π at the radius r^*.

For $L = 2$ and $\mathrm{Re} = 4000$, 3D spirals develop after the disturbance is superposed onto the axisymmetric flow previously described. The temporal behaviour exhibits now a quasi-periodic flow with two major frequencies equal to $\sigma = 0.9$ and $\sigma = 2.8$. Here four to five pairs of rolls are observed on the stationary disc, with a radial wavelength that remains close to $\lambda_r = \lambda_r^*/\delta = 25$. The rotating disc layer and the near-axis region remains unperturbed as in the axisymmetric solution, in agreement with the local Reynolds number criterion for the onset of the Ekman layer instability. The critical Reynolds number $\mathrm{Re}_{\delta c}$ is roughly 33 on the stationary disc, very close to the experimental criterion determined by Savas [14], $\mathrm{Re}_{\delta c} = 35$. During the transient period, axisymmetric patterns are also observed in the intermediate radial region corresponding to $33 \leq \mathrm{Re}_\delta \leq 63.5$ where the axisymmetric rolls immediately transform into spiral structures farther from the axis. The axisymmetric structures then vanish and only six spiral arms are observed after stabilization. The angle ε significantly decreases with the radius, $7^\circ \leq \varepsilon \leq 25.7^\circ$. The corresponding wavelengths vary over the range $16.1 \leq \lambda^*/\delta \leq 28.5$.

For $L = 5$ $\mathrm{Re} = 1600$, we observe the coexistence of stable circular and spiral patterns inside the Bödewadt layer as well as dislocation phenomena (Figure 1). The solution is time-dependent, with a dominant angular frequency nearly equal to the rotation frequency. Eight pairs of rolls of radial wavelength $8.8 \leq \lambda_r^*/\delta \leq 17$ decreasing with radius, move

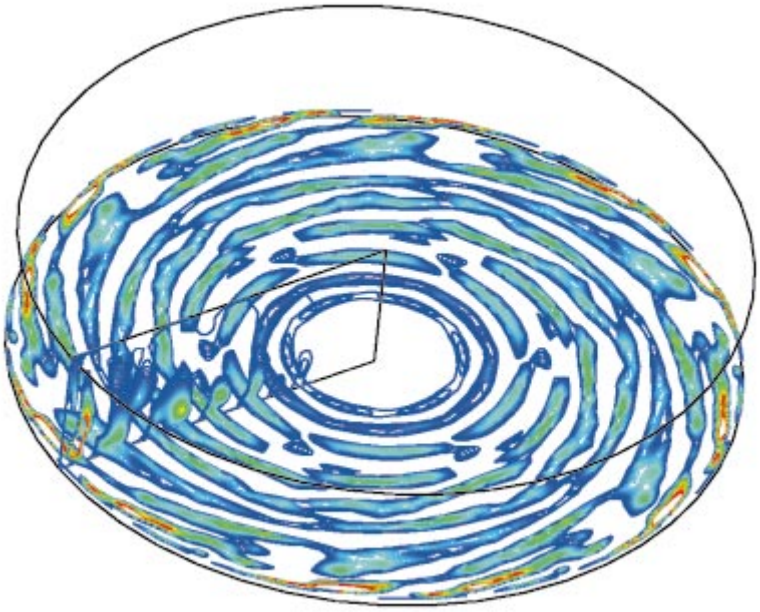

Figure 1. Co-existing annular and spiral patterns related to types II and I instabilities, respectively, of the Bödewadt layer. Isolines of the fluctuations of the axial component of the velocity in both $(r, -0.96, \phi)$ and $(r, z, \pi/4)$ planes. Cylindrical cavity $L = 5$, $\mathrm{Re} = 1600$

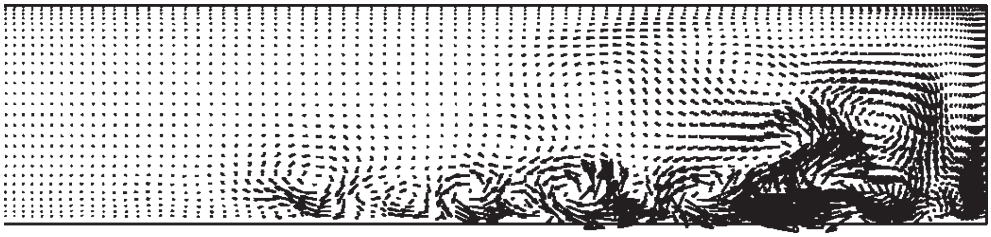

Figure 2. Projection of the fluctuating velocity field in the plane $(r, z, \pi/4)$ emphasizing the most unstable zone of the Bödewadt layer ($26.64 \leq \mathrm{Re}_\delta \leq 173$). Cylindrical cavity $L = 5$, $\mathrm{Re} = 1600$

downstream to $\mathrm{Re}_\delta = 26.64$ with phase velocity $-0.27 \leq V_\phi^*/\Omega r^* \leq -0.02$ (Figure 2). For $26.64 \leq \mathrm{Re}_\delta \leq 86.5$, five circular waves evolve. As in recent experiments [9, 15], spiral structures evolve at a larger distance from the axis, $86.5 \leq \mathrm{Re}_\delta \leq 173$, with angles varying as $7° \leq \varepsilon \leq 28°$; the spiral arms exhibit dislocations.

6. Linear stability theory results

We focus on the characteristics of these instabilities which are shown to be the most unstable. The onset of the type II instability in the *Bödewadt layer* (stator) has been found at $\mathrm{Re}_{\delta c\,\mathrm{II}} = 35.5$ with the wave angle $\varepsilon = 34.6°$, the wave number k components in radial and azimuthal directions $\alpha = \alpha^*\delta = 0.179$, $\beta = \beta^*\delta = 0.1237$ and the phase speed $V_\phi^*/\Omega r^* = \omega_r/k = -0.2526$ ($\sigma = \omega \mathrm{Re}_\delta$). The results have shown that type II instability can only exist in a narrow range of Re_δ, disappearing at $\mathrm{Re}_\delta = 68$. Type I instability occurs at $\mathrm{Re}_{\delta c\,\mathrm{I}} = 47.5$ with $\varepsilon = \tan^{-1}(\alpha/\beta) = -0.8°$, $\alpha = 0.2959$, $\beta = -0.00413$, $\lambda_r = 21.23$ and $V_\phi^*/\Omega r^* = -0.06175$. The exemplary isolines of the temporal amplification rate ω_i in the

plane of the wave angle and number (ε,k) obtained at the boundary layer of the stationary disc and also of the rotating disc are shown in Figure 3a and 3b, respectively. On the stationary disc, two separate regions of instability exist (Figure 3a) at $\mathrm{Re}_\delta = 65$. The first pick obtained for higher wave number with the maximum at $k \approx 0.28$ and $\varepsilon \approx -5°$ is identified as the type I instability. The second pick with maximum at $k \approx 0.2$ and $\varepsilon \approx 30°$ corresponds to the type II instability.

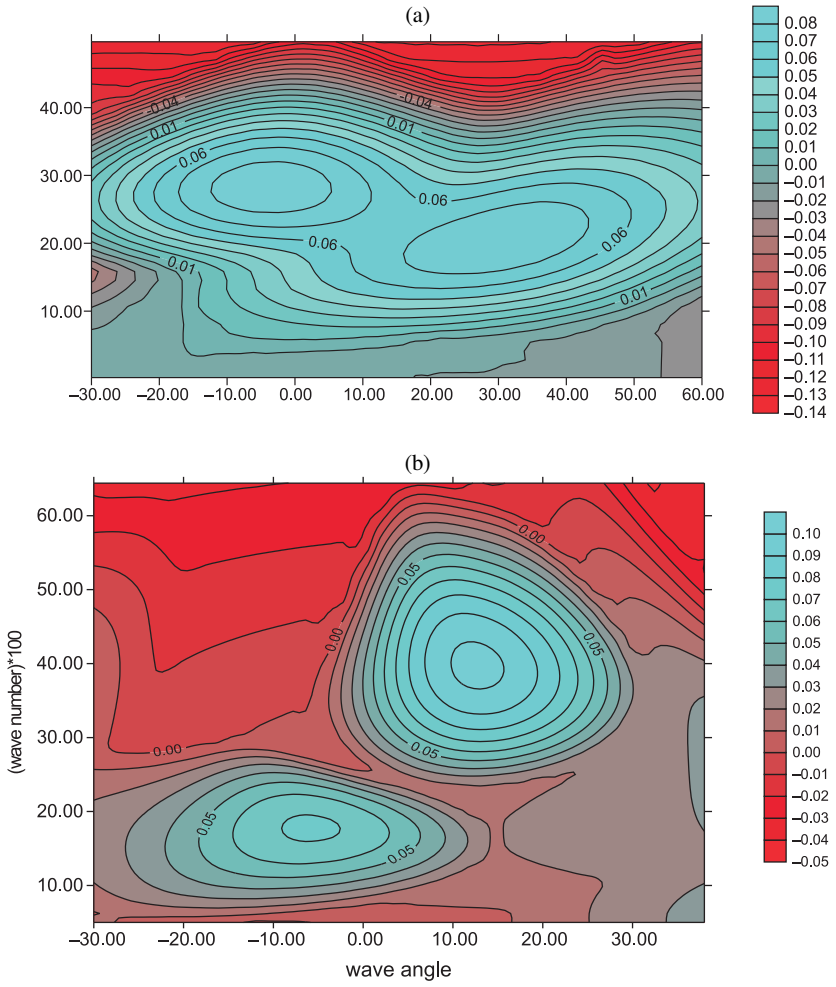

Figure 3. The isolines of $\omega_i = \text{const.}$: (a) stationary disc (Bödewadt layer), $\mathrm{Re}_\delta = 65$; (b) rotating disc (Ekman layer), $\mathrm{Re}_\delta = 400$

In the rotating disc flow, the onset of type II instability has been found in the present work at $\mathrm{Re}_{\delta c\,\mathrm{II}} = 90.23$ with $\varepsilon = -26.3°$, $\alpha = -0.1098$, $\beta = 0.22$ and $V_\phi^*/\Omega r^* = 0.39$. The type I instability occurs at $\mathrm{Re}_{\delta c\,\mathrm{I}} = 278.6$ with $\varepsilon = 10.9°$, $\alpha = 0.4173$, $\beta = 0.080322$ and $V_\phi^*/\Omega r^* = 0.0185$. Two separate regions of instability also on the rotating disc at $\mathrm{Re}_\delta = 400$ (Figure 3b). The first pick, obtained for the lower wave number with the maximum at $k = 0.177$ and $\varepsilon = -6.8°$, is identified as the type II instability. The second pick, with maximum at $k = 0.4$ and $\varepsilon = 12°$ corresponds to the type I instability.

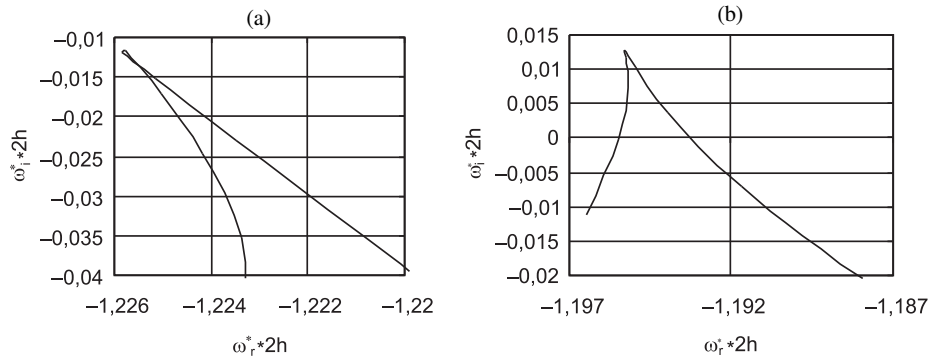

Figure 4. Temporal branches obtained for $\beta = -2.2$: (a) $\mathrm{Re}_\delta = 45$; (b) $\mathrm{Re}_\delta = 55$. Stationary disc

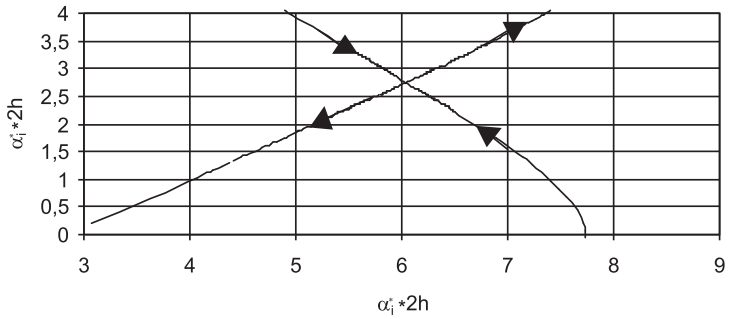

Figure 5. Spatial branch in α-plane: $\mathrm{Re} = 45$, $\beta = -2.2$. Stationary disc

Our linear stability results characterising the type I and type II instabilities are in very good agreement with Itoh's theoretical results [5] and also with the experimental results of Savas [14] who obtained $\mathrm{Re}_{\delta c\,\mathrm{II}} = 35.0$ in the case of the Bödsewadt layer. Itoh [5] gives for the same geometrical configuration: $\mathrm{Re}_{\delta c\,\mathrm{II}} = 38.6$, $\mathrm{Re}_{\delta c\,\mathrm{I}} = 48.1$ for the Bödewadt layer and $\mathrm{Re}_{\delta c\,\mathrm{I}} = 281$, $\mathrm{Re}_{\delta c\,\mathrm{II}} = 85.3$ for the Ekman layer. The type I instability critical parameters are also in good agreement with critical parameters obtained by Lingwood [9] for the stationary waves ($V_\phi^*/\Omega r^* = 0.0$) of the Ekman layer: $\alpha = 0.528$, $\beta = 0.14$, $\varepsilon = 14.5°$. However, there is a large difference between the present critical Reynolds number of the type I instability $\mathrm{Re}_{\delta c\,\mathrm{I}} = 278.6$ and that obtained for the Ekman boundary layer by Lingwood $\mathrm{Re}_{\delta c\,\mathrm{I}} = 116.3$. This discrepancy is probably due to influence of stationary disc in present investigation in contrast to the infinite domain in Ekman flow.

7. Convective/absolute instability

The Briggs [12] criterion with a fixed wave number in the spanwise direction β has been used in order to determine the region of absolute instability. In Figure 4, the exemplary temporal branches obtained on the stationary disc boundary layer for $\mathrm{Re} = 1000$, $\varepsilon = 45°$ (Figure 4a) $\mathrm{Re} = 55$ (Figure 4b) are displayed. The tip of a cusp like form indicates the pinch-point in the complex ω plane. If the imaginary part of ω in the tip of the cusp like form is positive $\omega_{oi} > 0$ (Figure 4b) the flow is absolutely unstable. In Figure 4b $\omega_{oi} = -0.0118$ and the flow is convectively unstable. The progression of the two spatial branches in α-plane given by the horizontal line $\omega_i = -0.0118$ for the wave angle $\varepsilon = 45°$ is shown in Figure 5. The arrows on the spatial branches indicate the direction of increasing ω_r.

Our LST results show that almost the whole boundary layer on the stationary disc is absolutely unstable. The critical Reynolds number of the absolutely unstable flow has been found at $\mathrm{Re}_{\delta ca} = 47.5$ with $\beta = -0.038$, $\alpha_r = 0.199$, $\alpha_i = 0.065$ and $\omega_r = -0.03$. The marginal curves for absolute and convective instability are shown in Figures 6a and 6b.

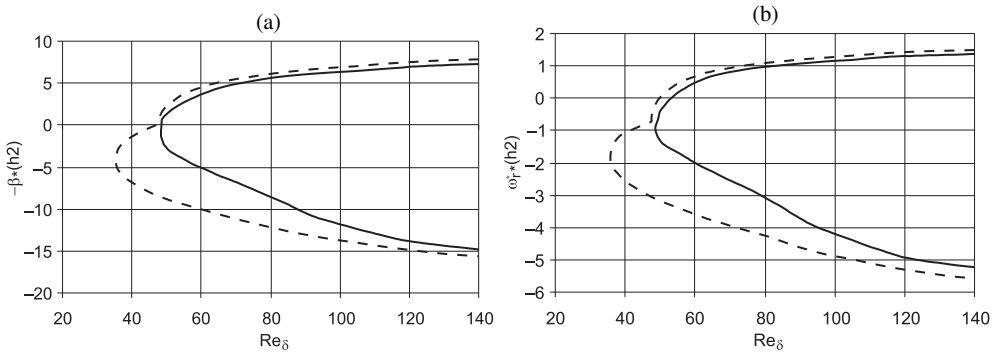

Figure 6. Marginal curves for absolute (——) and convective (– – –) instability. Stationary disk

On the rotating disc, the critical Reynolds number of the absolutely unstable flow found in the present analysis is $\mathrm{Re}_{\delta ca} = 578$ (with $\alpha_r = 0.2669$, $\alpha_i = -0.139$, $\beta = 0.158$, $\omega_r = -0.0284$).

These results complete the results of Lingwood [9] limited to the case of the flow over a single disc. Lingwood obtained $\mathrm{Re}_{\delta ca} = 21.6$, $\beta = -0.117$, $\alpha_r = 0.34$, $\alpha_i = 0.076$ and $\omega_r = -0.218$, for the Bödewadt layer, and $\mathrm{Re}_{\delta ca} = 198$, $\alpha_r = 0.379$, $\alpha_i = \pm 0.195$, $\beta = 0.184$, $\omega_r = \pm 0.0397$, for the Ekman layer.

8. Conclusions

Travelling stable circular waves have been observed for $\mathrm{Re}_\delta > 21$ ($L = 2$, $\mathrm{Re} = 4000$) and for $\mathrm{Re}_\delta > 27$ ($L = 5$, $\mathrm{Re} = 1600$). During the transient to a three-dimensional state ($L = 2$, $\mathrm{Re} = 4000$) circular patterns have also been temporarily obtained in the region corresponding to $33 < \mathrm{Re}_\delta < 63.5$. This range of Re_δ agrees well with the range where the type II instability is predicted to exist according to our LST (*i.e.* $35.5 < \mathrm{Re}_\delta < 68.0$). The annular waves immediately mute into three-dimensional spiral vortices for higher Re_δ where the type I instability is dominant according to the linear stability theory. The same good agreement between DNS and LST results have been found for a larger aspect ratio $L = 5$. In this case, both circular and spiral patterns are stable and coexist; circular waves of type II evolve in the range $26.6 < \mathrm{Re}_\delta < 86.5$ while type I spiral vortices expand at larger Re_δ. Moreover, very recent theoretical results [16] that are based on spatial non-parallel linear calculations and are devoted to the Bödewadt flow, also confirm that the annular structures near the stationary disc can be related to the type II instability. Indeed, the relevant parameters at the critical point, $\mathrm{Re}_{\delta c\,\mathrm{II}} = 19.8$, $\sigma = 2.1$ (*i.e.* $\omega = 0.106$), $\alpha = 0.482$, $\beta = 0.0$, $\varepsilon = 0.0°$, $V_\phi^*/\Omega r^* = -0.22$, determined by Feria [16], are very close to the characteristics obtained numerically. All these results are summarised in the Tables 1 and 2.

The DNS calculations show that the annular instability and the three-dimensional spirals only appear in the boundary layer of the stationary disc (Figure 2), while the boundary layer of the rotating disc remains entirely stable at least up to $\mathrm{Re}_\delta = 173$, which compares well with our present linear analysis.

Table 1. Characteristic parameters of the type II instability of the Bödewadt layer. Present DNS and LST results and literature results

Authors	Re_δ	ε	λ_r	$V_\phi^*/\Omega r^*$	$\mathrm{Re}_{\delta c\,\mathrm{II}}$	σ
Feria [16], PST	19.8	0.0°	12.3	−0.22	19.8	2.1
Itoh [5], LST	[38.6, 60]	[29.8°, 27°]	[34, 35.6]	[−0.23, −0.20]	38.6	—
Savas [14], Exp.	—	0.0°	19	−0.1	35	—
Present results, DNS, $L=2$	[21, 126.5]	0.0°	[10, 21]	[−0.08, −0.02]	21	0.9
Present results, DNS, $L=5$	[27, 173]	0.0°	[8, 17]	[−0.13, −0.21]	27	4
Present results, LST	[35.3, 60]	[34.6°, 31.3°]	[28.8, 30.5]	[−0.25, −0.23]	35.5	1.94

Table 2. Characteristic parameters of the type I instability of the Bödewadt layer. Present DNS and LST results and literature results

Authors	Re_δ	ε	λ_r	$V_\phi^*/\Omega r^*$	$\mathrm{Re}_{\delta c\,\mathrm{I}}$	σ
Itoh [5], LST	[48.1, 200]	[1.6°, −14°]	[23.7, 24.16]	[−0.077, −0.02]	48.1	—
Lingwood [9]	27.4	13.3°	13	0.0	27.4	—
Present results, DNS, $L=2$	[63.2, 126.5]	[7°, 25.7°]	[28.5, 16.1]	[−0.062, −0.68]	63.5	[0.9, 2.8]
Present results, DNS, $L=5$	[86.5, 173]	[7°, 28°]	[8.8, 17]	[−0.02, −0.27]	86.5	1
Present results, LST	[47.5, 200]	[−0.8°, −10°]	[21.2, 24.35]	[−0.062, −0.018]	35.5	0.9

The absolute instability regions are also theoretically identified. Our linear results show that the critical Reynolds numbers of the absolutely unstable flow are $\mathrm{Re}_{\delta ca} = 47.5$ and $\mathrm{Re}_{\delta ca} = 578$, for the Bödewadt and the Ekman layers, respectively. These results complete well the results of Lingwood [9] limited to the case of flow over a single disc and extend on the case of confined inter-disc flow and convectively unstable character of the Ekman layer type II instability, which will be the topic of a forthcoming paper.

The study on non-isothermal flows has shown that the thermal buoyancy effects induced by the rotational forces in a non-isothermal temperature field do alter the onset condition and the related critical parameters for this rotating mixed convection. The coupling nature of the flow and thermal characteristics results in a quite complicated physical phenomenon. Further study is worthwhile for its better understanding.

Acknowledgements

The computations were partly performed on the Cray J916 at Computer Center of Poznań.

References

[1] Kobayashi R, Kohama Y and Takamadate Ch 1980 *Acta Mechanika* **35** 71
[2] Lingwood R 1995 *J. Fluid. Mech.* **299** 17
[3] Lingwood R 1996 *J. Fluid. Mech.* **314** 373
[4] Daube O, Le Quéré P, Cousin R and Jacques R 2001 *Influence of Curvature on Transition Tounsteadiness and Chaos of Rotor/Stator Disk Flows* J. Fluid Mech. (submitted)
[5] Itoh M 1991 *ASME FED* **114** 83
[6] Tuliszka-Sznitko E and Soong C Y 2000 *Instability of Non-isothermal Flow between Coaxial Rotating Disks* Proc. European Congress on Computational Methods in Applied Sciences and Engineering, Barcelona
[7] Serre E, Crespo del Arco and Bontoux P 2001 *J. Fluid. Mech.* **434** 65
[8] Lilly D 1966 *J. Atmos. Sci.* **23** 481
[9] Lingwood R 1997 *J. Fluid. Mech.* **331** 405

[10] Gauthier P, Gondret P and Rabaud M 1999 *J.Fluid Mech.* **386** 105
[11] Serre E and Pulicani J 2001 *Computers and Fluids* **30** (4) (in print)
[12] Briggs R 1964 *Electron-Stream Interaction with Plasmas* MIT Press
[13] Kupfer K, Bers A and Ram A 1987 *Phys. Fluids* **30** 3075
[14] Savas O 1987 *J. Fluid Mech.* **183** 77
[15] Schouveiler L, La Gal P, Chauve M P and Takeda Y 1999 *Experiments in Fluids* **26** 179
[16] Feria F 2000 *Phys. Fluids* **12** (7) 1730